Highly Stretchable Polymer Composite with Strain-Enhanced Electromagnetic Interference Shielding Effectiveness

Bin Yao, Wei Hong, Tianwu Chen, Zhubing Han, Xinwei Xu, Renchao Hu, Jianyu Hao, Changhao Li, He Li, Steven E. Perini, Michael T. Lanagan, Sulin Zhang,* Qing Wang,* and Hong Wang*

Polymer composites with electrically conductive fillers have been developed as mechanically flexible, easily processable electromagnetic interference (EMI) shielding materials. Although there are a few elastomeric composites with nanostructured silvers and carbon nanotubes showing moderate stretchability, their EMI shielding effectiveness (SE) deteriorates consistently with stretching. Here, a highly stretchable polymer composite embedded with a three-dimensional (3D) liquid-metal (LM) network exhibiting substantial increases of EMI SE when stretched is reported, which matches the EMI SE of metallic plates over an exceptionally broad frequency range of 2.65–40 GHz. The electrical conductivities achieved in the 3D LM composite are among the state-of-the-art in stretchable conductors under large mechanical deformations. With skin-like elastic compliance and toughness, the material provides a route to meet the demands for emerging soft and human-friendly electronics.

Electromagnetic interference (EMI) is becoming ubiquitous due to widespread use of personal electronic devices and rising demands for increasingly powerful devices with improved functionality.[1,2] EMI can compromise performance of electronic devices by causing information leakage, false operations, or even complete failure.[1–3] There is also growing concern about detrimental effects of electromagnetic (EM) radiation, in particular from forthcoming 5th generation (5G) communications, on human health.[2] Typical materials used for mitigating EM transmission include sheet metals, metal screens, and metal foams.[1] Reflection and absorption of EM radiation represent two primary

mechanisms of EMI shielding, which arise from direct interaction of mobile charge carriers and electric/magnetic dipoles in shielding materials with the EM fields, respectively.[1,4] The electrical conductivity of the materials is regarded as the most critical parameter in governing the EMI shielding characteristics.[1]

Recently, a variety of electrically conductive fillers including metallic nanowires and nanoparticles,[2,5–7] liquid-metal (LM) droplets,[8–10] carbon-based materials (e.g., graphene, carbon fibers, and carbon nanotubes)[1,11,12] and 2D transition-metal carbides[13–15] have been incorporated into polymer matrix to yield EMI shielding polymer composites. While these composites are easily processable, lightweight, and mechanically flexible, their EMI shielding effectiveness (SE) is inevitably plagued by the reduction in electrical conductivity with the applied stretch,[6–8,12,15,16] a common phenomenon in the current stretchable conductors.[17–19] For example, the EMI SE of the LM based-composites decreases from ≈70 dB at 0% strain to ≈60 dB at 75% strain, and further to ≈35 dB at 300% strain.[8] A more than 60% drop in EMI SE is observed in the carbon nanotube-doped thermoplastic polyurethane under 200% strain.[12] Therefore, the development of highly stretchable EMI shielding materials with uncompromised performance are urgently needed in order to meet the emerging

B. Yao, X. Xu, J. Hao, Prof. H. Wang
State Key Laboratory for Mechanical Behavior of Materials
School of Material Science and Engineering
Xi'an Jiaotong University
Xi'an 710049, China
E-mail: wangh6@sustech.edu.cn
B. Yao, Z. Han, H. Li, Prof. Q. Wang
Department of Materials Science and Engineering
The Pennsylvania State University
University Park, PA 16802, USA
E-mail: wang@matse.psu.edu
Prof. W. Hong
Department of Mechanics and Aerospace Engineering
Southern University of Science and Technology
Shenzhen 518055, China

T. Chen, C. Li, Prof. S. Zhang
Department of Engineering Science and Mechanics
The Pennsylvania State University
University Park, PA 16802, USA
E-mail: suz10@psu.edu
R. Hu, Prof. H. Wang
Department of Materials Science and Engineering and Shenzhen
Engineering Research Center for Novel Electronic Information
Materials and Devices
Southern University of Science and Technology
Shenzhen 518055, China
S. E. Perini, Prof. M. T. Lanagan
Materials Research Institute
The Pennsylvania State University
University Park, PA 16802, USA

ADVANCED
SCIENCE NEWS
www.advancedsciencenews.com

ADVANCED
MATERIALS
www.advmat.de

demands for soft and human-friendly electronic devices, such as soft robotics, wearable electronics, flexible displays, and stretchable sensors.[20–27]

Here, we report that the EMI SE of the three-dimensional (3D) LM-skeleton-based polymer composite increases to more than double at 400% strain, which reaches the shielding levels of metallic plates measured under the same conditions. The increase of EMI SE originates from the greatly improved reflectivity and absorption of EM waves as a result of the stretch-induced enhancement of electrical conductivity and the increased surface-to-volume ratio, respectively, enabled by the 3D LM architecture. We demonstrate that the 3D LM composite displays a record electrical conductivity of 1.1×10^6 S m^{-1} at 400% strain[28–35] and robust electrical and EMI shielding performance under large repeated deformations. We investigate the EMI shielding properties of the composite over an unprecedented frequency range from 2.65–40 GHz that is relevant to 5G technology, in contrast to the relatively limited frequency region, that is, X-band (8.2–12.4 GHz), evaluated by the current EMI shielding materials.[1]

The preparation of the 3D LM composite begins with the synthesis of the eutectic gallium–indium alloy (EGaIn, 74.5% Ga and 25.5% In, by weight) microfoam using sugar cubes as the template and subsequent impregnation of porous EGaIn with silicone (Ecoflex 00-30, Smooth-On) (**Figure 1**a and Figures S1 and S2, Supporting Information). The composite can be scaled into different sizes and shaped into a variety of 3D geometries (Figure 1b,c and Figure S3, Supporting Information). Although the stretchable conductors were previously obtained by encapsulating LM into lithographically fabricated poly(dimethylsiloxane) (PDMS) nanonetworks, it required tediously repeated steps of photolithography to prepare 3D PDMS.[30] The computed micro-X-ray tomography (micro-CT, Figure 1d), scanning electron microscopy (SEM, Figure 1e) and optical microscopy (OM, Figure 1f) show that the 3D LM composite with 30 vol% LM consists of an interconnected LM skeleton with a typical diameter of 100 µm and continuous porous channels with an average pore size of 200 µm. Micro-CT confirms no obvious degradation in the 3D LM structure after stretching repeatedly to 200% strain for 10 000 cycles, indicative of its mechanical robustness and durability. (Figure 1g and Movie S1, Supporting Information). For comparison purpose, we also prepared the 0–3 LM composite with 30 vol% LM particles (15 µm in diameter), the 1–3 LM composite with 30 vol% LM fibers (12 µm in diameter and 70 µm in length),[36] and the composites with 5 vol% solid conductive fillers including graphene nanoplates (GNs), carbon nanotubes (CNTs), and $Ti_3C_2T_x$ (Supporting Information Section 2).

Tensile tests reveal that the 3D LM composite maintains a low elastic modulus of ≈30–60 kPa at a strain in the range of 0–400% and a fracture toughness of 2170 J m^{-2}, which are comparable to those of human skin (Figures S9 and S10,
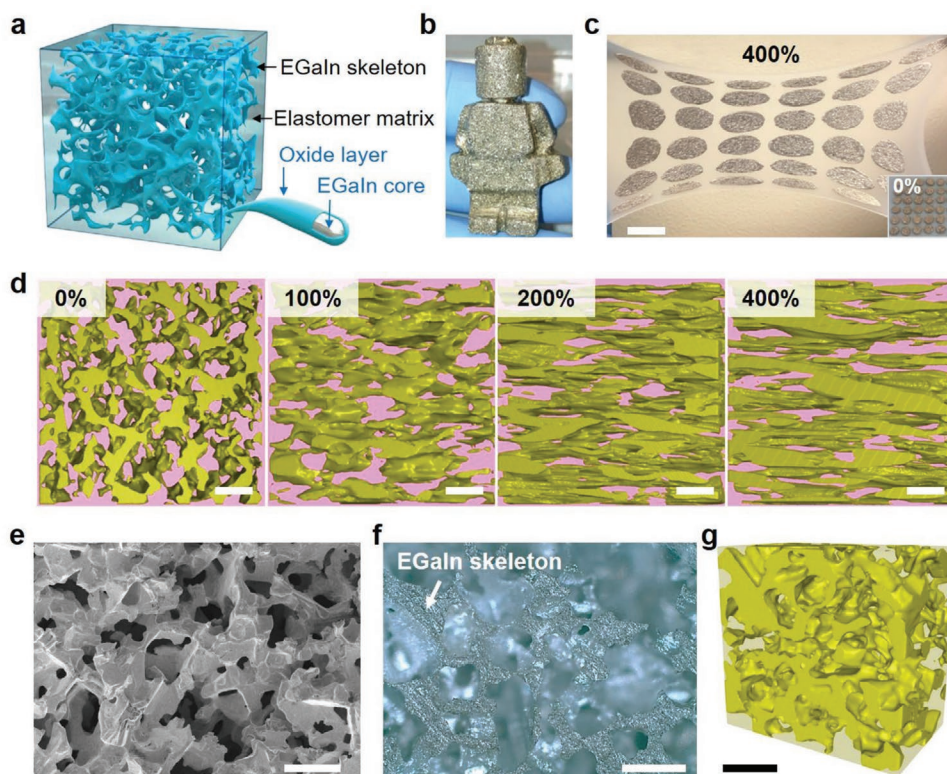
Figure 1. a) Schematic of the 3D LM composite. b) Photograph of the 3D LM composite shaped in a robot man solidified by iced-water. c) Photographs of a highly stretchable 3D LM composite film with patterns. Scale bar, 2 mm. d) The 3D reconstructed morphologies of the 3D LM composite by micro-CT at 0%, 100%, 200%, and 400% strain, respectively. Scale bar, 500 µm. e) SEM image of the 3D LM network before impregnation of silicone elastomer. Scale bar, 500 µm. f) Optical microscopy image of the 3D LM composite, in which the elastomer matrix is semitransparent. Scale bar, 500 µm. g) The 3D reconstructed structure of the 3D LM composite under 0% strain by micro-CT after 10 000 stretch-release cycles at 200% strain. Scale bar, 500 µm.

Supporting Information). We observed that the LM network can redistribute the applied load and dissipate energy by adapting their configurations through elongation and reorientation, presenting a large-scale, multimodal toughening mechanism similar to animal skins composed of fibril networks (Figure S10, Supporting Information).[37,38] The improved softness, stretchability (Figure S9, Supporting Information), and toughness of the composite by the LM network are in stark contrast to the composites with rigid fillers, which stiffen the composites and impair their stretchability.[17,18,29,39] Notably, the 3D LM composite exhibits considerably lower inelastic strain and superior recoverability to the 0–3 and 1–3 LM composites (Figures S11 and S12, Supporting Information). As shown in **Figure 2**a, after the first cycle at 400% strain, the inelastic strain in the 3–D LM composite is only 6.3%, in contrast to 33.9% and 24.5% inelastic strains of the 0–3 and 1–3 LM composites, respectively. The inelastic strain in the 3D LM composite changes negligibly over 50 cycles of loading–unloading under 300% strain, whereas it keeps increasing by 10.7% and 9.1%, respectively, in the 0–3 and 1–3 LM composites (Figure 2b).

The differences in the mechanical properties of the LM composites are attributable to the thin oxide layer (1–3 nm) natively grown on the LM surface upon exposure to air (Figure S13, Supporting Information).[40–42] First, the larger feature size and higher connectivity of the LM inclusions in the 3D composite correspond to a lower surface-to-volume ratio of the LM than those in the 0–3 and 1–3 composites. With the same LM volume fraction, the surface-to-volume ratio of the oxide layer in the 0–3 and 1–3 LM composites are ≈10 and ≈8.5 times greater, respectively, than that in the 3D LM composite, giving rise to higher elastic moduli of the 0–3 and 1–3 composites because of the relatively high stiffness of the oxide layer (Figure S9, Supporting Information). Second, the oxide layer is much more fragile than the elastomer matrix. Upon stretching, the oxide layer fractures, exposing fresh surface on which new oxide layer spontaneously forms; upon unloading, the restoring force again breaks the oxide layer, and the excess oxide fragments slide with each other. Both the processes involve energy dissipation and contribute to the inelastic strains in the composites. Because of the larger surface area of the oxide layer, the inelastic strains in the 0–3 and 1–3 LM composites are significantly higher than that in the 3D LM composite. We develop a comprehensive mechanics model to simulate the mechanical properties of the LM composites at large, cyclic stretch (Supporting Information, Section 5). The model invokes the Yeoh–Ogden–Roxburgh constitutive relations to capture the hyperelastic behavior and the damage evolution of the elastomer matrix. The LM inclusion is modeled as a nearly incompressible fluid with vanishing modulus, while the oxide layer as an elasto-plastic solid to mimic its inelastic deformation and energy dissipation upon cyclic loading. Indeed, the model predicts that the lower elastic modulus and inelastic strain of the 3D LM composite stem from its much less surface area of the oxide layer.

The electrical conductivity (σ) of the 3D LM composite in the loading direction increases monotonically with applied tensile strain, from 5.3×10^5 S m^{-1} under stretch-free condition to 1.1×10^6 S m^{-1} at 400% strain (Figure 2c). As compared in Figure 2e and Figure S16, Supporting Information, the 3D LM composite clearly outperforms most of the current stretchable conductors under large strains (>250%).[28–34] Upon stretching, the LM network elongates and rotates to align along the stretch direction, which is evidenced in the micro-CT images (Figure 1d, Figure S17, Supporting Information) and the projection analysis (Figure S18, Supporting Information). The rapid increase of the electrical conductivity along the stretch direction is ascribed to both stretch-induced alignment and elongation of LMs.[43] Our theoretical consideration reveals that for a representative LM wire with a tilt angle θ with respect to the stretch direction, stretch reduces its resistivity in the stretch direction by a factor $\alpha = \lambda^{-4}\sin2\theta + \cos^2\theta$, where $\lambda = 1 + \varepsilon$ is the stretch. This single factor also characterizes the stretch-induced alignment of the LM wire such that $\alpha^{1/2} = \cos\theta/\cos\theta'$, where θ' is the tilt angle of the wire after stretch (Supporting Information, Section 9). It is apparent that the larger the stretch λ, the higher level of the alignment, and the larger decrease in the resistivity. We further develop a computational model coupling large stretch with the electrical field to simulate stretch induced changes in conductivity, as shown in Figure 2d. The mechano–electrical model shows that the electric current takes a highly tortuous pathway between the two electrodes due to the highly spatial network of LM, as shown by the streamlines in Figure 2d. When stretched along the electric field direction, the segments of LM network are prone to rotation, reorientation, and elongation owing to their extreme flexibility, giving rise to alignment of the 3D LM skeleton in the stretching direction (Figure S21 and Movie S2, Supporting Information). The aligned and stretched segments form much straight pathways for the electric current, resulting in a higher effective conductivity.

On the other hand, the unstretched 0–3 and 1–3 LM composites are essentially electrical insulators, owing to the isolation of the low dimensional LM inclusions in the polymer matrix and the presence of insulation Ga$_2$O$_3$ layer on the surface of LMs.[44,45] Our mechano–electrical modeling shows that the electrical current concentrates at the tips of the stretched LM inclusions and thus enhances the conductivity of the adjacent polymer matrix, offering an additional mechanism of strain-enhanced conductivity in the 0–3 and 1–3 LM composites besides alignment and elongation of the LM inclusions (Figure S22, Supporting Information). Nevertheless, the σ of the stretched 0–3 and 1–3 LM composites, that is, 6×10^{-10} and 2.7×10^{-9} S m^{-1} measured at 10 kV m^{-1} and 1.5 kV m^{-1}, respectively, are 14–15 orders of magnitude lower than weak-field σ of the stretched 3D LM composite (Figures S19, Supporting Information). Opposite to the LM composites, the composites with solid fillers suffer from a steady decay in σ upon elongation, for example, from 3×10^{-3} S m^{-1} at the unstretched state to 1×10^{-4} S m^{-1} at 300% strain for the Ti$_3$C$_2$T$_x$-composite, owing to increased distance between conductive fillers (Figure 2c).[17,18] In addition, the composites with solid fillers are prone to interfacial decohesion because of large deformation incompatibility of the solid fillers and the polymer matrix, which breaks the electrically conductive path and yields reduced σ (Figure S23, Supporting Information).

We characterize the EMI SE of the composites in the frequency ranges of 2.65–5.95 GHz and 8.2–40 GHz within a waveguide method using a vector network analyzer. As presented in **Figure 3**a and Figures S25–S30, Supporting Information, a large enhancement in the average EMI SE is observed for
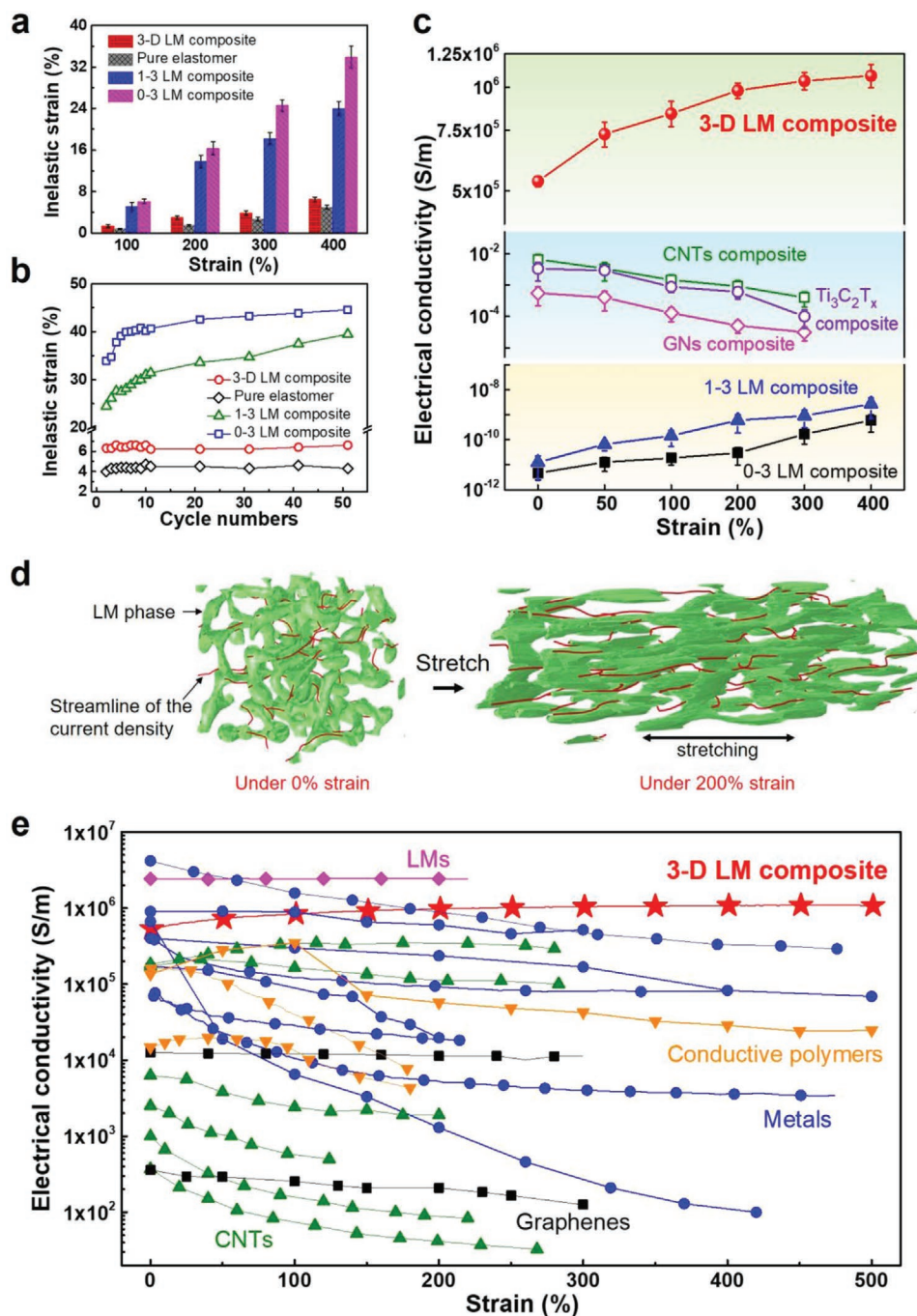
Figure 2. a) Inelastic strain after each was subjected to a cycle of varied maximum strain. b) Inelastic strain during multiple loading–unloading cycles. After the first cycle of loading–unloading at 400%, each was further stretched and released at 300% strain for 50 cycles. c) Electrical conductivity as a function of strain of the composites. d) The simulated 3D LM composite structure and the electric current (computed in the deformed geometry) when subject to a DC voltage under 0% and 200% strain, respectively. The red curves are the streamlines of the electric current density. The field of electric current density is much more aligned as indicated by the red streamlines. e) Electrical conductivity versus strain of the 3D LM composite and previous reported stretchable conductors. Each symbol indicates a set of materials as follows: liquid metal (pink diamond), silver (blue circle), CNT (green square), graphene (black up triangle), and conductive polymer (orange down triangle)-based composites. Detailed data of each point is presented in Table S1, Supporting Information. The error bars in (a) and (c) represent standard deviations obtained from at least three measurements using different samples.

the 3D LM composite when loading strains on the sample, for example, from 41.5 dB of 2.0 mm thick pristine film to 81.6 dB (highest value: 87 dB at 26.5 GHz) of 400% stretched film with

a thickness of 1.0 mm. In comparison, the current stretchable EMI shielding materials not only present limited stretchability (i.e., <300% strain) but also suffer from a dramatic decrease or

1907499 (4 of 7)
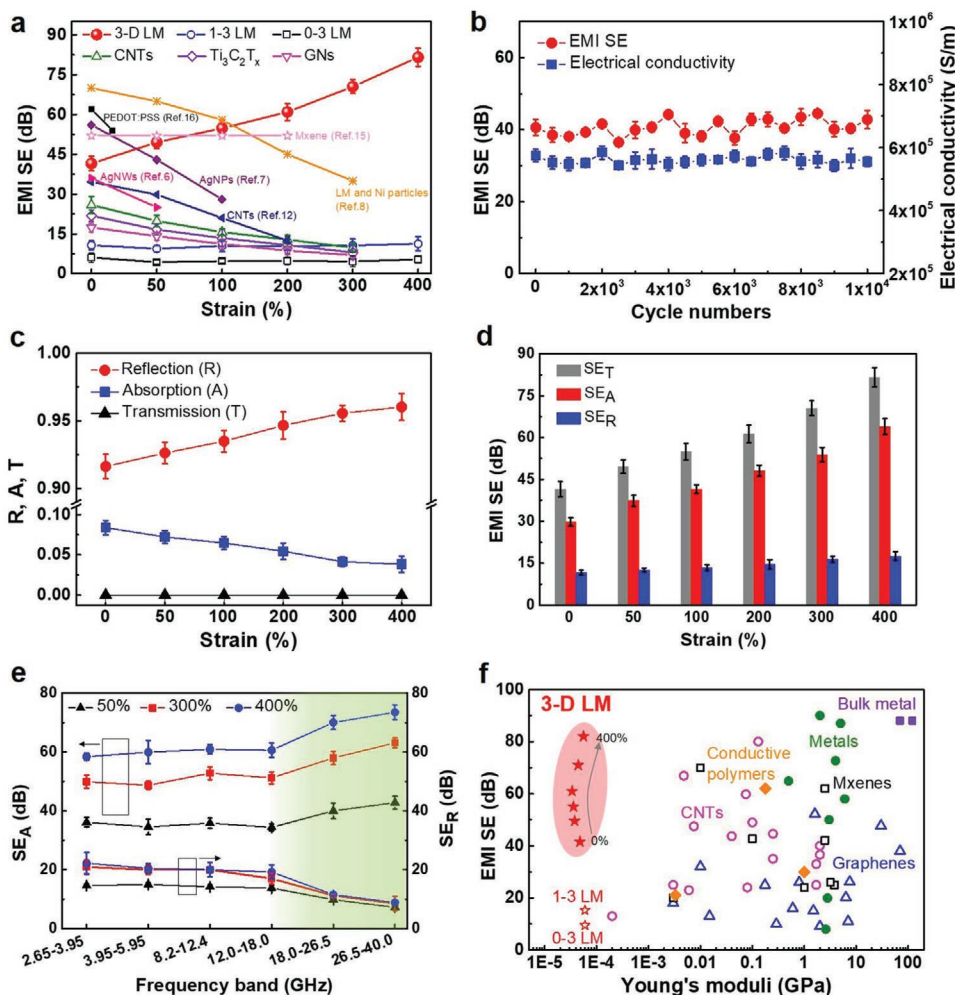
Figure 3. a) Average EMI SE versus strain of the composites in the frequency ranges of 2.65– 5.95 GHz and 8.2–40 GHz. Detailed data are presented in Table S2, Supporting Information. b) Electrical conductivity and EMI SE of 3D LM composite after 10 000 rigorous cycles of loading–unloading at 250% strain. c) Average reflection (R), absorption (A), transmission (T) and d) average SE$_T$, SE$_A$, SE$_R$ of the 3D LM composite at different strains in the frequency ranges of 2.65–5.95 GHz and 8.2–40.0 GHz. e) Frequency dependence of SE$_A$ and SE$_R$ of the 3D LM composite at various strains. f) Comparison of EMI SE and Young's modulus of the EMI shielding materials. Each symbol indicates a set of materials as follows: 3D LM composite (red solid stars), 1–3 LM and 0–3 LM composites (red open stars), conductive polymer (orange solid diamonds), bulk metals (purple solid squares), MXenes (black open squares), CNTs (pink open circles), and graphenes (blue open triangles). Detailed data of each point are presented in Table S4, Supporting Information. The error bars from (a–e) represent standard deviations obtained from at least three measurements using independent samples.

an invariant in EMI SE when stretched (Figure 3a, and Table S2, Supporting information).[6–8,12,15,16] We also measure Al and Cu plates with a thickness of 1 mm under the same conditions and conclude that their EMI SE values are around 88 dB (Figure S31, Supporting Information). This indicates that the highly stretched 3D LM composite reaches the shielding efficiency (>99.999999%, Table S3, Supporting Information) of traditional metal plates with the same thickness. This finding is striking because the stretching process is accompanied with a continuous decrease of film thickness, which is known to reduce EMI SE.[1,13] Indeed, as shown in Figure S32, Supporting Information, the EMI SE of the composites shows a strong positive correlation with film thickness regardless of filler structures. For instance, the average EMI SE of the unstretched 3D LM composite is reduced from 55.7 to 29.8 dB at 8.2–12.4 GHz by decreasing film thickness from 3.0 to 1.2 mm. To better

illustrate the influence of strain on EMI SE, we assess the EMI SE of the composites with the same film thickness. As shown in Figure S33, Supporting Information, for the 1.6 mm thick 3D LM composite film, the average EMI SE increases progressively with strain, for example, from 34.5 dB at 0% strain to 86.2 dB (highest value: 88.3 dB) at 400% strain measured at 8.2–12.4 GHz. Apparently, the contribution of strain-induced changes of electrical properties and composite microstructure outweighs the loss derived from the decreased thickness and thus improves the overall EMI SE. Notably, the 3D LM composite gives highly stable σ and EMI SE even after 10 000 rigorous stretch-release cycles at 250% strain, further manifesting its high mechanical and electrical durability under repeated strain (Figure 3b and Figure S34, Supporting Information).

By contrast, no obvious change in the EMI SE of the 0–3 and 1–3 LM composite is observed, which remains around 5 and

10 dB, respectively, with increasing strain. As a result of rapidly reduced σ with strain, the composites filled with GNs, CNTs, and $Ti_3C_2T_x$ present dramatic decreases in EMI SE, for example, from 17.4, 25.9, and 21.9 dB to 7, 9.8, and 8 dB, respectively, when the strain increases from 0% to 300%, which are in agreement with previously reported results (Figures S25–S30, Supporting Information).[6,12]

We analyze the contributions from absorption (SE_A) and reflection (SE_R) to the total EMI SE to elucidate the shielding mechanism of the 3D LM composite. As shown in Figure 3c, the reflection of EM wave is increased from 0.916 under stretch-free condition to 0.960 under 400% strain, indicating that 8.4% of incident EM waves are attenuated to 4.0% as the composite is stretched. Accordingly, SE_R is increased from 11.6 to 17.5 dB. The strong reflection is ascribed to the strain-enhanced σ and the aligned LM skeletons in the plane perpendicular to the incident EM wave direction. As presented in Figure 3d, a systematic increase is observed in SE_A during extension, for example, from 29.7 dB of pristine sample at 0% strain to 63.9 dB under 400% strain. This rise in SE_A is related to the stretch-increased surface-to-volume ratio of the 3D LM composite. As characterized by micro-CT and confirmed by theoretical calculation (Figure S35, Supporting Information), the average diameter of the LM skeletons decreases from 100 to 55 µm when the sample is stretched to 400% strain, which leads to an 82% increment in the surface-to-volume ratio of the composite. The 3D LM architecture introduces abundant conductive surfaces and facilitates multiple reflection/scattering and subsequent absorption of the EM waves inside the LM network. Since EM absorption mainly occurs on the surface of the LM as suggested by the skin depth effect, the stretch-increased surface-volume fraction ratio results in much more multiple reflections of the EM waves, and consequently, gives rise to an improvement in the absorption of EM waves.[2,4] While the total EMI SE of the 3D LM composite shows little variation with frequency, a trend of decrease in SE_R and increase in SE_A with increasing frequency, especially above 18 GHz, is observed (Figure 3e and Figure S36, Supporting Information). The penetration of EM wave is known to increase with decreasing wavelength, especially when the dimension of the material approaches 0.01λ (λ: wavelength of EM radiation).[3] For the 3D LM composite, the characteristic dimension of the elastomer region is around 200 µm, which corresponds to 0.01 λ of 15 GHz. Therefore, we observe a rapid drop in the reflection at ≈18 GHz. The increase of SE_A with frequency arises from the continuous decrease of the skin depth of LM, for example, from 5.4 µm at 2.65 GHz to 2.7 µm at 10 GHz and 1.3 µm at 40 GHz, at high frequencies.[46]

We further demonstrate proof-of-concept applications of the 3D LM composite used as stretchable conductors (Figure S37, Supporting Information) and EMI shields in wireless power transmission systems at 27 MHz, 2.4 GHz, 10.5 GHz, and 60 GHz (Figures S38–S41, Movies S3–S6, Supporting Information). As shown in Figure 3f, the 3D LM composite exhibits unique EMI SE and Young's modulus when compared to currently available EMI shielding materials. With an unprecedented combination of metal-like EMI shielding capability, unusual strain-enhanced electrical conductivity, outstanding stretchability, skin-compatible mechanical properties, and facile preparation, our material can fill an important gap in the stretchable materials that are indispensable to soft electronics.

Supporting Information

Supporting Information is available from the Wiley Online Library or from the author.

Conflict of Interest

The authors declare no conflict of interest.

[1] H. Abbasi, M. Antunes, J. I. Velasco, *Prog. Mater. Sci.* **2019**, *103*, 319.

[2] X. C. Tong, *Advanced Materials and Design for Electromagnetic Interference Shielding*, CRC Press, Boca Raton, FL, USA **2009**.

[3] D. R. J. W. J. L. Norman Violette, M. F. Violette, *Electromagnetic Compatibility Handbook*, Springer, New York **1985**.

[4] D. D. L. Chung, *Carbon* **2001**, *39*, 279.

[5] Q. Zhang, Q. Liang, Z. Zhang, Z. Kang, Q. Liao, Y. Ding, M. Ma, F. Gao, X. Zhao, Y. Zhang, *Adv. Funct. Mater.* **2018**, *28*, 1703801.

[6] J. Jung, H. Lee, I. Ha, H. Cho, K. K. Kim, J. Kwon, P. Won, S. Hong, S. H. Ko, *ACS Appl. Mater. Interfaces* **2017**, *9*, 44609.

[7] Z. Liu, F. Wan, L. Mou, M. Jung de Andrade, D. Qian, R. Wang, S. Yin, K. Li, H. Chen, B. An, Z. Hu, H. Wang, M. Zhu, S. Fang, Z. Liu, *Adv. Electron. Mater.* **2019**, *5*, 1800817.

[8] M. Zhang, P. Zhang, Q. Wang, L. Li, S. Dong, J. Liu, W. Rao, *J. Mater. Chem. C* **2019**, *7*, 10331.

[9] X. Li, M. Li, J. Xu, J. You, Z. Yang, C. Li, *Nat. Commun.* **2019**, *10*, 3514.

[10] M. Ou, W. Qiu, K. Huang, S. Chu, *J. Appl. Phys.* **2019**, *125*, 134906.

[11] Q. Song, F. Ye, X. Yin, W. Li, H. Li, Y. Liu, K. Li, K. Xie, X. Li, Q. Fu, L. Cheng, L. Zhang, B. Wei, *Adv. Mater.* **2017**, *29*, 1701583.

[12] D. Feng, D. Xu, Q. Wang, P. Liu, *J. Mater. Chem. C* **2019**, *7*, 7938.

[13] F. Shahzad, M. Alhabeb, C. B. Hatter, B. Anasori, S. M. Hong, C. M. Koo, Y. Gogotsi, *Science* **2016**, *353*, 1137.

[14] J. Liu, H. B. Zhang, R. Sun, Y. Liu, Z. Liu, A. Zhou, Z. Z. Yu, *Adv. Mater.* **2017**, *29*, 1702367.

[15] Y. Li, X. Tian, S. P. Gao, L. Jing, K. Li, H. Yang, F. Fu, J. Y. Lee, Y. X. Guo, J. S. Ho, P. Y. Chen, *Adv. Funct. Mater.* **2019**, *30*, 1907451.

**ADVANCED
SCIENCE NEWS**
www.advancedsciencenews.com

**ADVANCED
MATERIALS**
www.advmat.de

[16] P. Li, D. Du, L. Guo, Y. Guo, J. Ouyang, *J. Mater. Chem. C* **2016**, *4*, 6525.

[17] N. Matsuhisa, X. Chen, Z. Bao, T. Someya, *Chem. Soc. Rev.* **2019**, *48*, 2946.

[18] M. L. Hammock, A. Chortos, B. C. Tee, J. B. Tok, Z. Bao, *Adv. Mater.* **2013**, *25*, 5997.

[19] J. A. Rogers, T. Someya, Y. Huang, *Science* **2010**, *327*, 1603.

[20] D. H. Kim, N. Lu, R. Ma, Y. S. Kim, R. H. Kim, S. Wang, J. Wu, S. M. Won, H. Tao, A. Islam, K. J. Yu, T. I. Kim, R. Chowdhury, M. Ying, L. Xu, M. Li, H. J. Chung, H. Keum, M. McCormick, P. Liu, Y. W. Zhang, F. G. Omenetto, Y. Huang, T. Coleman, J. A. Rogers, *Science* **2011**, *333*, 838.

[21] Q. Hua, J. Sun, H. Liu, R. Bao, R. Yu, J. Zhai, C. Pan, Z. L. Wang, *Nat. Commun.* **2018**, *9*, 244.

[22] J. Liang, L. Li, X. Niu, Z. Yu, Q. Pei, *Nat. Photonics* **2013**, *7*, 817.

[23] W. Gao, S. Emaminejad, H. Y. Y. Nyein, S. Challa, K. Chen, A. Peck, H. M. Fahad, H. Ota, H. Shiraki, D. Kiriya, D. H. Lien, G. A. Brooks, R. W. Davis, A. Javey, *Nature* **2016**, *529*, 509.

[24] S. I. Rich, R. J. Wood, C. Majidi, *Nat. Electron.* **2018**, *1*, 102.

[25] M. Kubo, X. Li, C. Kim, M. Hashimoto, B. J. Wiley, D. Ham, G. M. Whitesides, *Adv. Mater.* **2010**, *22*, 2749.

[26] G. Zhang, P. Zhao, X. Zhang, K. Han, T. Zhao, Y. Zhang, C. K. Jeong, S. Jiang, S. Zhang, Q. Wang, *Energy Environ. Sci.* **2018**, *11*, 2046.

[27] T. Someya, Z. Bao, G. G. Malliaras, *Nature* **2016**, *540*, 379.

[28] S. Choi, S. I. Han, D. Jung, H. J. Hwang, C. Lim, S. Bae, O. K. Park, C. M. Tschabrunn, M. Lee, S. Y. Bae, J. W. Yu, J. H. Ryu, S. W. Lee, K. Park, P. M. Kang, W. B. Lee, R. Nezafat, T. Hyeon, D. H. Kim, *Nat. Nanotechnol.* **2018**, *13*, 1048.

[29] Y. Kim, J. Zhu, B. Yeom, M. Di Prima, X. Su, J. G. Kim, S. J. Yoo, C. Uher, N. A. Kotov, *Nature* **2013**, *500*, 59.

[30] J. Park, S. Wang, M. Li, C. Ahn, J. K. Hyun, D. S. Kim, D. K. Kim, J. A. Rogers, Y. Huang, S. Jeon, *Nat. Commun.* **2012**, *3*, 916.

[31] Y. Wang, C. Zhu, R. Pfattner, H. Yan, L. Jin, S. Chen, F. Molina-Lopez, F. Lissel, J. Liu, N. I. Rabiah, Z. Chen, J. W. Chung, C. Linder, M. F. Toney, B. Murmann, Z. Bao, *Sci. Adv.* **2017**, *3*, e1602076.

[32] N. Matsuhisa, D. Inoue, P. Zalar, H. Jin, Y. Matsuba, A. Itoh, T. Yokota, D. Hashizume, T. Someya, *Nat. Mater.* **2017**, *16*, 834.

[33] B. Y. Ahn, E. B. Duoss, M. J. Motala, X. Guo, S. I. Park, Y. Xiong, J. Yoon, R. G. Nuzzo, J. A. Rogers, J. A. Lewis, *Science* **2009**, *323*, 1590.

[34] T. Sekitani, H. Nakajima, H. Maeda, T. Fukushima, T. Aida, K. Hata, T. Someya, *Nat. Mater.* **2009**, *8*, 494.

[35] S. Liang, Y. Li, Y. Chen, J. Yang, T. Zhu, D. Zhu, C. He, Y. Liu, S. Handschuh-Wang, X. Zhou, *J. Mater. Chem. C* **2017**, *5*, 1586.

[36] R. E. Newnham, D. P. Skinner, L. E. Cross, *Mater. Res. Bull.* **1978**, *13*, 525.

[37] W. Yang, V. R. Sherman, B. Gludovatz, E. Schaible, P. Stewart, R. O. Ritchie, M. A. Meyers, *Nat. Commun.* **2015**, *6*, 6649.

[38] N. Kazem, M. D. Bartlett, C. Majidi, *Adv. Mater.* **2018**, *30*, 1605985.

[39] N. Matsuhisa, M. Kaltenbrunner, T. Yokota, H. Jinno, K. Kuribara, T. Sekitani, T. Someya, *Nat. Commun.* **2015**, *6*, 7461.

[40] A. Zavabeti, J. Z. Ou, B. J. Carey, N. Syed, R. Orrell-Trigg, E. L. H. Mayes, C. Xu, O. Kavehei, A. P. O'Mullane, R. B. Kaner, K. Kalantar-Zadeh, T. Daeneke, *Science* **2017**, *358*, 332.

[41] M. D. Dickey, R. C. Chiechi, R. J. Larsen, E. A. Weiss, D. A. Weitz, G. M. Whitesides, *Adv. Funct. Mater.* **2008**, *18*, 1097.

[42] N. Kazem, T. Hellebrekers, C. Majidi, *Adv. Mater.* **2017**, *29*, 1605985.

[43] C. Thrasher, Z. Farrell, N. Morris, C. Willey, C. Tabor, *Adv. Mater.* **2019**, *31*, 1903864.

[44] H. Wang, Y. Yao, Z. He, W. Rao, L. Hu, S. Chen, J. Lin, J. Gao, P. Zhang, X. Sun, X. Wang, Y. Cui, Q. Wang, S. Dong, G. Chen, J. Liu, *Adv. Mater.* **2019**, *31*, 1901337.

[45] C. Pan, E. J. Markvicka, M. H. Malakooti, J. Yan, L. Hu, K. Matyjaszewski, C. Majidi, *Adv. Mater.* **2019**, *31*, 1900663.

[46] V. C. P. R.B. Schulz, D.R. Brush, *IEEE Trans. Electromagn. Compat.* **1988**, *30*, 187.